Influence of Basic Red 1 dye adsorption on thermal stability of Na-clinoptilolite and Na-bentonite

D. Sternik · M. Majdan · A. Deryło-Marczewska ·
G. Żukociński · A. Gładysz-Płaska ·
V. M. Gun'ko · S. V. Mikhalovsky

Abstract Influence of physically adsorbed basic red 1 (BR1) dye on the physicochemical properties of natural zeolite (clinoptilolite) and clay (bentonite) was compared using adsorption, FTIR, and TG/DTA methods. A larger adsorption of the dye was observed for bentonite (0.143 mmol/g) than for clinoptilolite (0.0614 mmol/g) per gram of an adsorbent. However, the adsorption values are the same per surface unit (1.8 μmol/m^2). The result (per gram) is due to location of dye molecules in interlayer and interparticle space of bentonite with much larger specific surface area than that of clinoptilolite. The dye adsorption leads to a decrease in the specific surface area and the pore volume of both minerals. The adsorption changes also a character of active sites and thermal stability. A TG study shows that the dye adsorption on bentonite changes adsorbed water amounts, weight loss, and decomposition temperature. In the case of zeolite, the dye adsorption insignificantly influences the thermal stability. The dehydration energy distributions calculated from the Q-TG and Q-DTG data demonstrate a complex mechanism of water thermodesorption and the influence of adsorbed dye on this process.

Introduction

Such aluminosilicates as natural zeolites and clays are the most popular cheap adsorbents widely applied in industry, environment protection, agriculture, medicine, optics, microelectronics and many other fields [1–5]. The sieve-molecular properties, availability of strongly active surface sites, high resistance to acids and other useful properties of zeolites allow the use of them as catalysts in cracking, hydrocracking, isomerization and other processes. Aluminosilicate catalysts are characterized by high activity, good selectivity, stability and capability of multiple regeneration. They are also used for purification of wastewater from heavy metal salts and other pollutants. Conventional technologies of removal of wastewater dyes such as coagulation, flocculation, biodegradation and oxidation are expensive and often ineffective [6, 7]. Therefore, recent studies have been focused on application of clays as low-cost adsorbents to remove colored pollutants [8–11]. In this aspect, interaction of natural minerals with water and organics is of importance [11–13].

Bentonite and clinoptilolite are natural minerals composed of the aluminosilicate matrix with a variety of embedded other metal oxides and metal cations [14–16]. Bentonite is highly colloidal and plastic clay which basic structural unit is composed of two tetrahedrally coordinated sheets of silicon ions surrounding a sandwiched octahedrally coordinated sheet of aluminum ions. Isomorphous substitution of Al^{3+} for Si^{4+} by in the tetrahedral sheets and Mg^{2+} or Fe^{2+} for Al^{3+} in the octahedral sheets results in the negative surface charge of bentonite. Clinoptilolite includes 3D system of channels of four types. Three types of them are formed

D. Sternik (✉) · M. Majdan · A. Deryło-Marczewska ·
G. Żukociński · A. Gładysz-Płaska
Chemistry Faculty, Maria Curie-Sklodowska University,
3 M. Curie-Sklodowska Sq, 20-031 Lublin, Poland
e-mail: dsternik@poczta.umcs.lublin.pl

V. M. Gun'ko
Chuiko Institute of Surface Chemistry,
17 General Naumov Street, 03164 Kiev, Ukraine

V. M. Gun'ko · S. V. Mikhalovsky
School of Pharmacy & Biomolecular Sciences,
University of Brighton, Lewes Road, Brighton BN2 4GJ, UK

by 8-membered rings, and the fourth one is of 10-membered rings. The net negative surface charge of aluminosilicates is counterbalanced by monovalent (Na^+, K^+) and divalent (Ca^{2+}) cations [17, 18].

There are several types of reactions of dyes with clays [19] such as colored π- and d-complexes formation and ion-exchange, acid–base and oxidation–reduction reactions. The aim of this article is to show the effects of adsorption of rhodamine 6G as a representative dye on the physicochemical properties of aluminosilicates (clinoptilolite, bentonite) that are of importance from both theoretical and practical points of view.

Experimental

Materials

Two aluminosilicates (i) natural zeolite [Transcarpathian clinoptilolite, Clin, with the general formula of ($K_{2.3}Na_{0.5}$ $Ca_{2.1}Mg_{0.6}Fe(III)_{0.9}Fe(II)_{0.2}Ti_{0.2})(Si_{31.4}Al_{6.5}O_{44}) \cdot 21.8H_2O$ and the chemical composition (in %): SiO_2, 67.29; TiO_2, 0.26; Al_2O_3, 12.32; Fe_2O_3, 1.26; FeO, 0.25; MgO, 0.29; CaO, 3.01; Na_2O, 0.66; K_2O, 2.76; H_2O, 10.90, whereby the content of the main mineral is $85 \pm 6\%$], and (ii) clay [bentonite, Ben, O, 54.2%, Na, 2.7%, Mg, 1.9%, Al, 11.2%, Si, 27.5%, Fe, 2.4%, cation exchange capacity CEC = 0.79 mmol/g (Sigma-Aldrich)] were used as the initial materials. Basic Red 1, BR1, Rhodamine 6G (Sigma-Aldrich, C.I. = 45160, $C_{28}H_{31}N_2O_3Cl$, FW = 479.01] used is a cationic dye.

Modification

On preparation of Na-clinoptilolite and Na-bentonite by ion-exchange reaction, 5 g of native solids (particle fraction

>0.1 mm) were added to 100 ml of 1 M NaCl solution and stirred for 4 h. After aging for 24 h, the samples were filtered, washed several times with water, dried and ground. Dye-modified minerals were prepared by physical adsorption of BR1 at 25 °C. The BR1 solutions (100 ml) of a certain concentration (0.001 M—BR1-L; 0.002 M—BR1-H) were shaken with 1 g of Na-bentonite or Na-clinoptilolite, and then the samples were filtered in 24 h.

Methods

The thermogravimetric (TG) measurements were carried out using a derivatograph Q-1500D (MOM, Hungary). The TG, differential TG (DTG) and differential thermal analysis (DTA) curves were recorded over the 20–950 °C range at a heating rate of 10 °C/min in the static air atmosphere using a platinum crucible (sample weight 100 mg, reference Al_2O_3). The thermal analysis was also performed in quasi-isothermal conditions recording the Q-TG and Q-DTG weight loss as a function of temperature and time over the 20–200 °C range at a constant heating rate of 6 °C/min [20].

The specific surface area calculated using the BET method [21] (Table 1, S_{BET}) and the pore volume (V_p) were determined from low-temperature nitrogen adsorption measured using a Micrometrics ASAP 2405 V1.01 analyzer. Before measurements the samples were degassed at 170 °C. The pore size distributions (PSDs) were calculated using two methods. The first one is based on a self-consisting regularization procedure (SCRP) applied to a mixture model with slitshaped (alumina or silica) and cylindrical pores and voids between spherical silica particles (SCSCV) [22]. The SCRP allows us to estimate contributions (Table 1, c_i values) of pores of different types to the total porosity and the specific surface area. The SCRP convergence was fast because the difference in the c_i

Table 1 Structural characteristics of unmodified and modified aluminosilicates

Sample	$S_{BET}/$ $m^2\,g^{-1}$	$V_p/$ $cm^3\,g^{-1}$	$V_{mic}/$ $cm^3\,g^{-1}$	$V_{mes}/$ $cm^3\,g^{-1}$	$V_{mac}/$ $cm^3\,g^{-1}$	$S_{mic}/$ $m^2\,g^{-1}$	$S_{mes}/$ $m^2\,g^{-1}$	$S_{mac}/$ $m^2\,g^{-1}$	$R/$ nm	Δw	c_{slit}	c_{cyl}	c_{void}
Clin-Na	34	0.144	0.003	0.093	0.050	4.3	26.6	2.7	7.1	0.335	0.40	0.48	0.12
Clin-BR1-H	25	0.106	0.0	0.072	0.035	0.5	22.8	1.8	7	0.482	0.33	0.31	0.36
Ben-Na	80	0.163	0.014	0.132	0.024	27.7	51.3	1.0	3.7	0.422	0.69	0.12	0.19
Ben-Na[a]	80	0.163	0.012	0.130	0.027	24.2	54.5	1.2	3.7	0.398	0.52	0.22	0.26
Ben-Na[b]	80	0.163	0.018	0.106	0.046	38.4	39.8	1.8	3.7	−0.145	0	1	0
Ben-BR1-H	37	0.116	0.0	0.109	0.011	0.1	36.8	0.3	5.5	0.121	0.76	0.06	0.18

S_{BET} BET specific surface area, V_p the pore volume, R hydraulic radius of pores, S_{mic}, S_{mes}, and S_{mac} are the specific surface area and V_{mic}, V_{mes}, and V_{mac} are the pore volume of micro-, meso-, and macropores, respectively, Δw is the deviation of the pore shape from the model of a mixture of slitshaped and cylindrical pores and voids between spherical particles

[a] Slitshaped pores with alumina, others with silica

[b] Cylindrical pores in silica

values for the 9th and 10th steps was typically small $|\Delta c_i| \leq 0.00002$. The second method is based on nonlocal density functional theory (NLDFT) with the model of cylindrical pores in silica [23] (Quantachrome Instruments software, version 1.51). For better view, the differential PSDs ($f_V(R) \sim dV/dR$, $f_S(R) \sim dS/dR$) were recalculated into incremental PSDs (IPSDs) $\phi_i = (f_i + f_{i+1})(R_{i+1} - R_i)/2$. To estimate the pore model quality, a criterion

$$\left(\Delta w = \frac{S_{BET}}{\int_{R_{min}}^{R_{max}} f_S(R)dR} - 1 \right)$$

[24] of the deviation of the pore shape from the model was used. Contributions of micropores (pore radius $R < 1$ nm), mesopores ($1 < R < 25$ nm) and macropores ($R > 25$ nm) (Table 1) were estimated integrating $f_V(R)$ (for volume components) and $f_S(R)$ (surface area) obtained with the SCSCV method.

The amount of an adsorbed dye modifier was determined using elemental analysis. The types of functionalities of the materials and adsorbed species were determined on the basis of the infrared spectroscopy. The FT-IR spectra of aluminosilicates were recorded in the transmission mode at room temperature on 1725X Perkin-Elmer instrument using KBr pellet technique (1:20) with the resolution 2 cm^{-1} according to procedure given in [25]. The KBr was dried in drier at 200 C during 24 h, then 560 mg KBr was homogenized with the zeolite sample in ball grinder (produced by Narva Brand-Erbisdorf DDR) The tablets (radius 1 cm, thickness 0.1 cm were prepared using hydraulic press.

Results and discussion

Figure 1 presents the nitrogen adsorption/desorption isotherms measured at 77.4 K for (a) Na-clinoptilolite and (b) Na-bentonite unmodified and modified by adsorbed dye. Clinoptilolite and bentonite are characterized by not large V_p and S_{BET} values (Table 1) that are typical for natural minerals. The shape of the isotherms corresponds to a certain superposition of isotherms of II and IV types of the IUPAC classification without plateau adsorption. The shapes of nitrogen adsorption isotherms on unmodified and BR1-loaded clinoptilolite samples are very similar. The effect of adsorbed dye molecules on pore characteristics of clinoptilolite is rather weak. Relatively narrow hysteresis loops and substantial fraction of mesopores in total pore volume (Table 1) suggest mesoporous character of pore structure. Small adsorption over the range of low relative pressures confirms small contribution of microporosity (Table 1). High increase of adsorption for relative pressures over 0.8 corresponds to adsorption in macropores. In the case of bentonite the shapes of isotherms measured for the unmodified and dye-modified samples are also similar. However, decrease of nitrogen adsorption for the sample loaded with BR1 evidences strong changes of porosity (Table 1) due to preadsorbed dye molecules. The IPSDs of both minerals are broad with several peaks (Fig. 2). These features reflect a complex texture of the natural minerals with pores of different types and shapes which also have a complex chemical composition of the walls. Therefore, the model of cylindrical pores, which is poorly appropriate for clays, overestimates the microporosity of Ben-Na (Table 1, S_{mic}, V_{mic}) and $\Delta w < 0$. Therefore, a complex model of pores as a mixture of slitshaped and cylindrical pores and voids between nanoparticles was applied. The use of this model with slitshaped pores with alumina slightly changes the pore type composition (Table 1, c_i) and the IPSD (Fig. 2c) of Ben-Na. However, the changes in the IPSD shape are insignificant (because of the oxygen/OH outer layer in silica and alumina). Therefore, silica (as the main component of both minerals studied) was used in other models for all types of pores (Table 1; Fig. 2).

Both aluminosilicates have broad IPSD (Fig. 2). However, the zeolite does not practically have micropores in contrast to the clay, but relative contribution of macropores is higher for clinoptilolite (Fig. 2; Table 2), as well as contribution of

Fig. 1 Nitrogen adsorption–desorption isotherms for unmodified (*black line*) and modified by BR1 solutions (0.002 M) (*broken line*) for Na-clinoptilolite (**a**) and Na-bentonite (**b**) samples
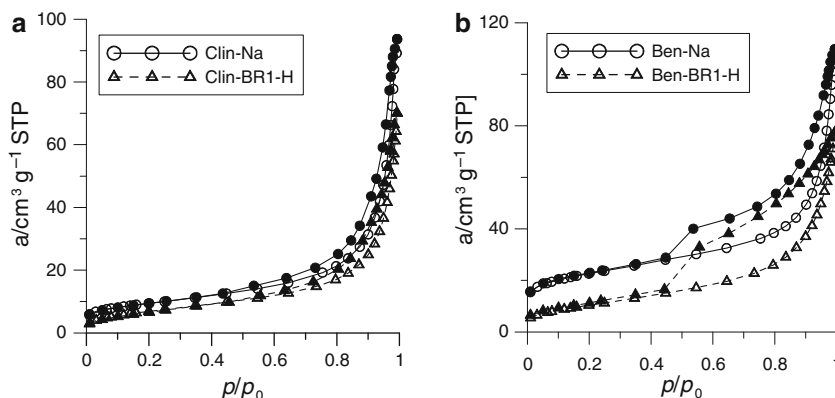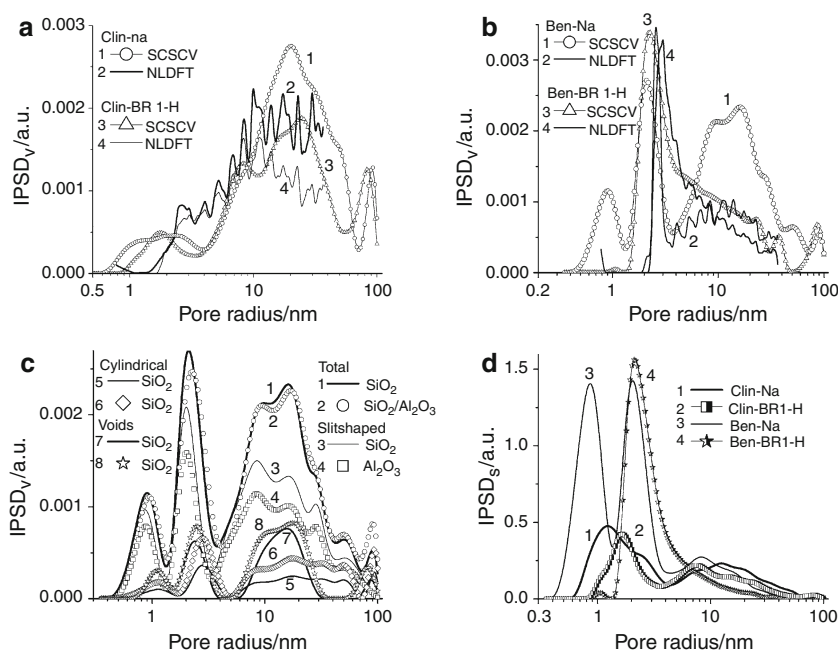
Table 2 The vibrational bands in FTIR spectra of BR1 samples

FTIR/cm^{-1}			Assignment [38–40]
BR1	Clin-BR1-H	Ben-BR1-H	
732	–	740	C–H out of plane bending of xanthene ring
1315	1305	1306	Xanthene ring stretching vibrations
1365	1367	1367	C–N stretching vibrations
1501	1504	1504	Xanthene ring stretching vibrations
1536	1533	1536	Xanthene ring C–C stretching vibrations
1608	1612	1612	Xanthene ring stretching vibrations
1647	1647	1652	Xanthene ring C–C stretching vibrations
1715	1714	1723	Phenyl group vibrations
2868	2874	2877	CH$_2$ symmetric stretching vibrations
2974	2982	2979	CH$_2$ asymmetric stretching vibrations

cylindrical pores (c_{cyl}). Contributions of slitshaped pores and voids between tiny particles are larger for bentonite (Table 1, c_{slit}, c_{void}). This is due to the structural nature of clay and zeolite studied and a smaller size of primary particles of the clay than the zeolite. For the latter, the pore size distribution is more heterogeneous with the main contribution of mesopores at $R > 4$ nm (Fig. 2a, d) because of textural features of natural zeolites [26]. Bentonite has a broad IPSD too, but there is a narrow high IPSD$_V$ peak at $R = 2$–3 nm (Fig. 2b) and two narrow IPSD$_S$ peaks (Fig. 2d).

Adsorption modification of the adsorbents by organic compounds depends on their porosity, PSD, number and type of surface active sites, energetic heterogeneity of the surface, etc. Binding of a cationic dye by aluminosilicates is due to the hydrogen bonds and can also lead to ion-exchange reactions. A greater adsorption of rhodamine R6G per gram of bentonite (0.143 mmol/g) than that of clinoptilolite (0.0614 mmol/g) is due to a larger specific surface area of the former, since the adsorption per surface area unit is the same for both (1.8 μmol/m^2). Thus, one can conclude that monolayer surface coverage with dye is formed on both adsorbents. In the case of the clay, the dye molecules can locate in interlayer space (slitshaped micropores and narrow mesopores, Fig. 2) and interparticle textural pores (which can be modeled by cylindrical pores and voids between neighboring clay particles) [27]. The initial zeolite has pores of different shapes (Figs. 1 and 2, Table 1) but with the main contribution of cylindrical pores (c_{cyl}). The nitrogen adsorption/desorption isotherms for the unmodified and modified samples are close (Fig. 1), but the structural characteristics, especially related to narrow pores, drop down after the modification with dye (Table 1, Fig. 2). This is a result of the monolayer adsorption of the dye molecules in all pores but with a greater effect for narrow pores with a larger portion of the volume occupied by the dye molecules. This leads to certain textural changes (Figs. 1, 2; Table 1). Similar changes were observed in the case of the modification of silica gels by coal deposits [28, 29], proteins [30], and organosilanes [31, 32].

In the case of the modified clay, pores at $R < 1.5$ nm disappear (Fig. 2b, d) because of, at least, two effects. The first one is completely filling of narrow pores by the dye

molecules. The second one is broadening of narrow pores due to intercalation by the dye molecules. In addition, the IPSD shape of broad pores changes due to rearrangement of secondary clay particles and changes in the textural meso- and macroporosity. Notice that the contribution of slitshaped pores (as narrow mesopores) increases for the modified clay (Table 1, c_{slit}) because of the intercalation effect. A decrease in contribution of narrow and broad pores is observed for modified zeolite (Fig. 2a, d). However, relative changes of the IPSD and the structural characteristics for the zeolite are much smaller than that for the clay due to a higher rigidity of clinoptilolite particles and smaller the S_{BET} value (i.e., smaller monolayer capacity for adsorbed dye).

Aluminosilicate samples were studied using the FTIR method. In the case of aluminosilicates (Fig. 3a, c) four characteristic groups of IR bands are observed [7, 33–37] and assigned to: lattice vibrations below 400 cm^{-1} and pseudo-lattice vibrations at about 500–700 cm^{-1}, internal vibrations Si–O(Si) and Si–O(Al) in tetrahedral or alumino- and silico-bridges in at 400–1200 cm^{-1}, and bands of adsorbed water and surface hydroxyls are at about 1630–1650 and 3000–3800 cm^{-1}, respectively. The FTIR spectra of dye-modified samples have contributions of the xanthene rings and methylene groups (Fig. 3b, d; Table 2). This is the evidence of the modification of aluminosilicates with dye. The intensity of these bands depends on the quantity of adsorbed rhodamine 6G. In the case of modified clay, organic cations change intensity and position of water bands at 3000–4000 cm^{-1}. The band at 3442 cm^{-1} for the latter has a higher intensity than the band at 3436 cm^{-1} in the initial sample. Therefore, one can conclude that water
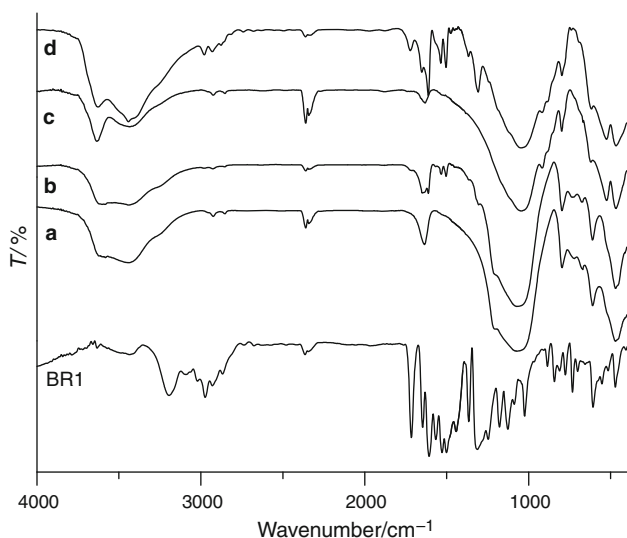
is less strongly hydrogen bonded due to the displacement by the dye molecules from surface adsorption sites [34].

Figure 4 shows the TG and DTG curves for rhodamine 6G indicating that thermo-oxidation of the solid BR1 occurs in two main stages. The first endothermic process below 150 °C corresponds to removal of physically adsorbed water from dye particles. According to the literature [27], the second oxidation process at 200–700 °C may be divided into three stages: (IIa) 170–270 °C, a melting and dehydration with a peak at 253 °C; (IIb) 270–380 °C, partial oxidation of the H atoms of the dye with a peak at 345 °C; and (IIc) thermo-oxidation of the H, N atoms and carbonized residue at 380–700 °C.

The adsorption of the dye molecules on the adsorbent surface changes not only the textural characteristics of the materials (Figs. 1, 2; Table 1) but also a character of their active sites and thermal stability (Figs. 4, 5, 6). The TG, DTG, and DTA curves are compared for initial aluminosilicates and the samples with adsorbed rhodamine 6G (Figs. 5, 6). In the case of unmodified Na-bentonite two endothermic peaks are observed. The first weight loss of 9%, with a minimum at about 97 °C, is due to removal of adsorbed and interlayer water [41–43]. The second peak from 500 to 750 °C is due to dehydroxylation as an endothermic process with the weight loss of 6%.

The DTA curves of bentonite modified by BR1 are shown in Fig. 5b–c. The DTG curves can be divided into three parts [19, 44, 45]: (1) a low-temperature region (<170 °C) where the clay loses adsorbed and interlayer water, (2) a central region (170–500 °C) with an exothermic peak at 396 °C assigned to the decomposition of the dye

Fig. 3 FTIR spectra of unmodified and modified aluminosilicates: **a** Clin-Na; **b** Clin-BR1-H; **c** Ben-Na; and **d** Ben-BR1-H
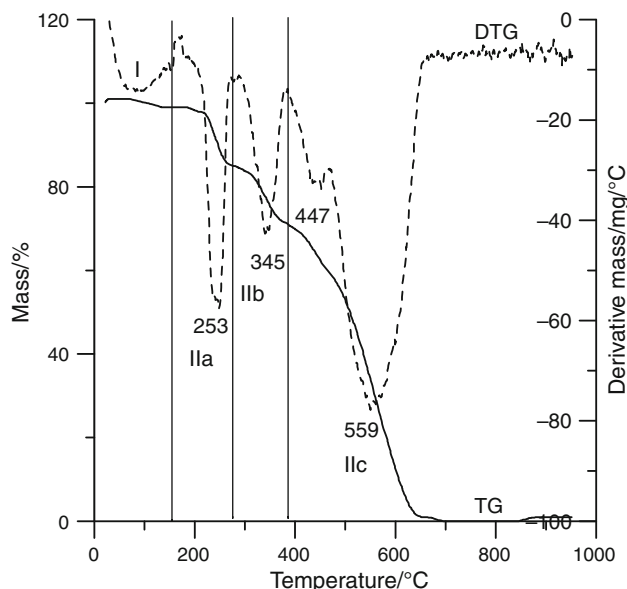

Fig. 4 TG and DTG curves for rhodamine 6G heated in the static air atmosphere
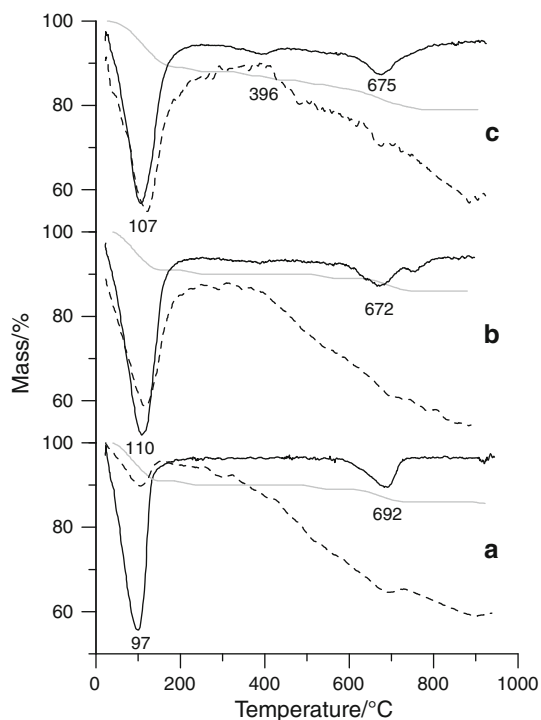
Fig. 5 TG (*gray line*), DTG (*black line*), and DTA (*broken line*) curves for bentonite samples: **a** Na-bentonite, **b** Ben-BR1-L, and **c** Ben-BR1-H

Fig. 6 TG (*gray line*), DTG (*black line*), and DTA (*broken line*) curves of clinoptilolite samples: **a** Na-clinoptilolite, **b** Clin-BR1-L, and **c** Clin-BR1-H

molecules, and (3) a high-temperature region (>500 °C), where dehydroxylation of bentonite and pyrolysis of charcoal are observed. The BR1 adsorption on the bentonite surface leads to changes in the weight loss and a significant shift of decomposition temperature. In comparison to the initial sample, a larger peak located at about 107 °C at the weight loss of 11% means that the samples with the adsorbed BR1 are more humid and contain more physisorbed water. Below 500 °C, the weight loss corresponds to a partial thermo-oxidation of organic hydrogen. This step is characteristic for decomposition of the majority of organic compounds [46, 47]. This process depends on chemical composition and the amounts of adsorbed organics, the clay surface properties, and adsorbate–adsorbent interactions [45]. The dye adsorption also leads to the displacement of the maximum of the main DTG peak on the third stage toward lower temperatures ($\Delta T \sim 18$ °C). It can be characteristic for the dye molecules adsorbed in the interlayer space of clay particles.

In the case of Na-clinoptilolite, two stages are observed on the thermal analysis in the 20–950 °C range (Fig. 6a) at the total weight loss of 12%. The first weight loss of 7% at a minimum at about 92 °C is due to desorption of physically adsorbed water. The second stage occurs at 300–700 °C because of dehydroxylation (i.e., associative desorption of water molecules on removal of the surface hydroxyls). These data are in good
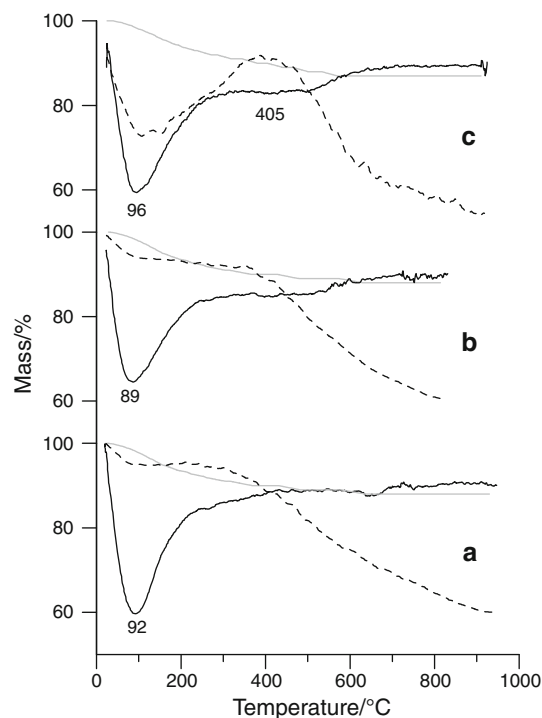
correlation with previous results [18]. Dye adsorption does not significantly influence the thermal stability of the modified zeolite (Table 3) because of its high structural stability and rigidity and the absence of rearrangement of particles due to the dye adsorption observed for the modified clay.

For better illustration of the process on the first stage (water removal), the thermal analysis of aluminosilicates was performed in quasi-isothermal conditions. From the Q-TG and Q-DTG curves (Fig. 7), the dehydration energy distribution function $Q(E_d)$ was determined using the formula [48]:

$$-\frac{1}{1-\theta_i}\frac{d\theta_i}{dT} = \frac{v_i}{\beta}\exp\left(-\frac{E_i}{R_g T}\right) \quad (1)$$

where: $T = T_o + \beta t$, θ is the degree of surface coverage, v is the entropy factor, E_i is the desorption energy calculated for each temperature, T_o and T are the initial and given temperatures of desorption, respectively, β is the heating rate, t the time, and R_g the universal gas constant and

$$Q(E_d) = -\frac{d\theta}{dT}\frac{1}{T} \quad (2)$$

The dependence $Q(E_d)$ for bentonite samples (Fig. 8a) has a regular shape of the Gauss curve type. The E_d values are in the range 20–75 kJ mol^{-1} for the initial sample and

Table 3 Thermal behavior of studied samples

Samples	DTG peak/°C	Exo↑/endo↓	Weight loss/% at temperature/°C			Total weight loss/%
			20–200	200–400	400–900	
Na-Clin	92	↓	7	3	2	12
Clin-BR1-L	79	↓	7	4	3	14
Clin-BR1-H	96; 405	↓; ↑	6	4	3	13
Na-Ben	97; 692	↓; ↓	9	0	6	15
Ben-BR1-L	110; 672	↓; ↓	12	1	6	19
Ben-BR1-H	107; 396; 675	↓; ↑; ↓	11	2	8	21
BR1	137; 253; 282; 345; 447; 559	↓; ↑; ↑	2	28	70	100

Fig. 7 Q-TG and Q-DTG curves of water thermodesorption from bentonite (**a**) and clinoptilolite (**b**) samples
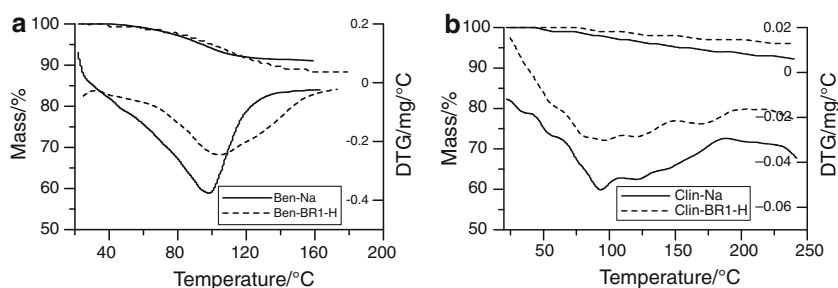
Fig. 8 Dehydration energy distribution for unmodified and modified bentonite (**a**) and clinoptilolite (**b**)
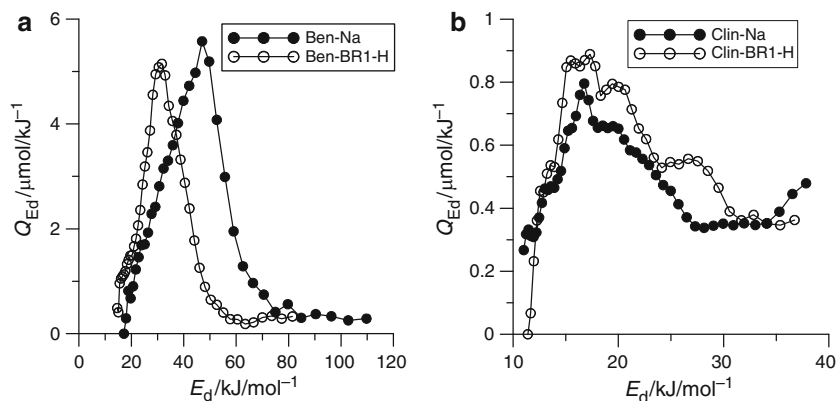
20–60 kJ mol^{-1} for Ben-BR1-H. The E_d value of the $Q(E_d)$ maximum for the BR1 modified clay shifts toward lower energy (about 15 kJ mol^{-1}). This indicates a decrease in water-BR1-adsorbent interactions in comparison with water-Ben-Na. This effect can be caused by larger amounts of physisorbed water and competitive adsorption of organic cations and water molecules on the same surface sites.

In the case of zeolite, $Q(E_d)$ corresponds to a broad curve with a few maxima at 17, 19, and 27 kJ mol^{-1} for Clin-BR1-H and a curve with two maxima for unmodified clinoptilolite. This suggests a complex thermodesorption mechanism of water and the influence of adsorbed dye on this process. However, these changes are relatively small because the BR1 adsorption on clinoptilolite is small.

Conclusions

(1) The adsorption of basic red 1 dye on clinoptilolite and bentonite is due to the formation of the hydrogen bonds between surface hydroxyls and dye molecules with participation of water molecules.

(2) The dye adsorption leads to the decrease in the specific surface area and the porosity of aluminosilicates and changes in the pore size distribution over total pore size range.

(3) The thermal decomposition of dye/clinoptilolite samples indicates the external surface character of dye molecules sorption.

(4) Changes in the structural characteristics and features of the thermal decomposition of unmodified and

modified bentonite samples indicate the sorption of dye molecules in the interlayer space of the mineral.

(5) For both minerals, the adsorption of dye per surface area unit is the same and corresponds to the monolayer coverage of the surfaces.

References

1. Chuah GK, Xu X, Zhan P, Joenicke S. Catalysts from MCM-41: framework modification. pore size engineering, and organic-inorganic hybrid materials. J Mol Catal A. 2002;181:25–31.

2. Bartea L, Kouwanhoven HW, Prins R. Vapour-phase nitration of benzene over modified mordenite catalysts. Appl Catal A. 1995; 129:229–50.

3. Xiubin H, Zhanbin H. Zeolite application for enhancing water infiltration and retention in loess soil. Resour Conserv Recycl. 2001;34:45–52.

4. Gladysz-Plaska A, Kowalska-Ternes M, Majdan M. Adsorption of toxic metal ions on zeolites. Przem Chem. 2000;79:298.

5. Mumpton FA, Fishman RH. The application of natural zeolites in animal science and aquaculture. J Anim Sci. 1997;45:1188–203.

6. Slokar YM, Majcen Le Marechal AM. Methods of decoloration of textile wastewaters. Dyes Pigments. 1998;37:335–56.

7. Crini G. Non-conventional low-cost adsorbents for dye removal: A review. Bioresour Technol. 2006;97:1061–85.

8. Bagane M, Guiza S. Removal of a dye from textile effluents by adsorption. Ann Chim Sci Mater. 2000;25:615–26.

9. Wang Ch-C, Juang L-Ch, Hsu T-Ch, Lee Ch-K, Lee J-F, Huang F-Ch. Adsorption of basic dyes onto montmorillonite. J Colloid Interface Sci. 2004;273:80–6.

10. Juang RS, Wu FC, Tseng RL. The ability of activated clay for the adsorption of dyes from aqueous solutions. Env Technol. 1997; 18:525–31.

11. Dragoi B, Rakic V, Dumitriu E, Auroux A. Adsorption of organic pollutants over microporous solids investigated by microcalorimetry techniques. J Therm Anal Calorim. 2010;99:733–40.

12. Clausen P, Signorelli M, Schreiber A, Hughes E, Plummer CJG, Fessas D, Schiraldi A, Månson J-AE. Equilibrium desorption isotherms of water, ethanol, ethyl acetate, and toluene on a sodium smectite clay. J Therm Anal Calorim. 2009;98:833–41.

13. Halim NA, Ibrahim ZA, Ahmad AB. Intercalation of water and guest molecules within Ca^{2+}—montmorillonite DSC studies in low temperature range. J Thermal Anal Calorim. 2010. doi: 10.1007/s10973-010-0860-3.

14. Bergaya F, Theng BKG, Lagaly G, editors. Handbook of clay science. Elsevier, Amsterdam; 2006.

15. Özcan A, Ömeroğlu Ç, Erdoğan Y, Özcan AS. Modification of bentonite with a cationic surfactant: an adsorption study of textile dye Reactive Blue 19. J Hazard Mater. 2007;140:173–9.

16. Eren E, Afsin B. An investigation of Cu(II) adsorption by raw and acid-activated bentonite: a combined potentiometric. thermodynamic, XRD, IR, DTA study. J Hazard Mater. 2008;151:682–91.

17. Yener J, Kopac T, Dogu G, Dogu T. Adsorption of Basic Yellow 28 from aqueous solutions with clinoptilolite and amberlite. J Colloid Interface Sci. 2006;294:255–64.

18. Korkuna O, Leboda R, Skubiszewska-Zięba J, Vrublevs'ka T, Gun'ko VM, Ryczkowski J. Structural and physicochemical properties of natural zeolites: Clinoptilolite and mordenite. Microporous Mesoporous Mater. 2006;87:243–54.

19. Yariv S, Cross H, editors. Organo-clay complexes and interactions. New York: Marcel Dekker; 2002. pp 39–111.

20. Paulik F. Special trends in thermal analysis. Chichester: Wiley; 1995.

21. Brunauer S, Emmett PH, Teller E. Adsorption of gases in multimolecular layers. J Am Chem Soc. 1938;60:309–19.

22. Gun'ko VM. Consideration of the multicomponent nature of adsorbents during analysis of their structural and energy parameters. Theor Exp Chem. 2000;36:319–24.

23. Ravikovitch PI, Neimark AV. Characterization of nanoporous materials from adsorption and desorption isotherms. Colloids Surf A. 2001;187–188:11–21.

24. Gun'ko VM, Mikhalovsky SV. Evaluation of slitlike porosity of carbon adsorbents. Carbon. 2004;42:843–9.

25. Majdan M, Kowalska-Ternes M, Pikus S, Staszczuk P, Skrzypek H, Zięba E. Vibrational and scanning electron microscopy study of the mordenite modified by Mn, Co, Ni, Cu, Zn and Cd. J Mol Struct. 2003;649:279–85.

26. Hernández MA, Corona L, Rojas F. Adsorption characteristics of natural erionite, clinoptilolite and mordenite zeolites from Mexico. Adsorption. 2000;6:33–45.

27. Landau A, Zaban A, Lapides I, Yariv S. Montmorillonite treated with rhodamine-6G mechanochemically and in aqueous suspensions. J Therm Anal Calorim. 2002;70:103–13.

28. Gun'ko VM, Leboda R, Charmas B, Villieras F. Characterization of spatial and energetic structures of carbon-silica gels. Colloids Surf A. 2000;173:159–69.

29. Gun'ko VM, Leboda R, Marciniak M, Grzegorczyk W, Skubiszewska-Zięba J, Malygin AA, Malkov AA. CVD-titania/silica gel carbonized due to pyrolysis of cyclohexene. Langmuir. 2000;16:3227–43.

30. Sternik D, Staszczuk P, Pękalska J, Grodzicka G, Gawdzik B, Osypiuk-Tomasik J, Witer P. Surface properties of silica gel samples modified by selected proteins. J Therm Anal Calorim. 2006;86:85–91.

31. Kruk M, Jaroniec M, Gilpin RK, Zhou YW. Nitrogen adsorption studies of coated and chemically modified chromatographic silica gels. Langmuir. 1997;13:545–50.

32. Jaroniec CP, Kruk M, Jaroniec M, Sayari A. Tailoring surface and structural properties of MCM-41 silicas by bonding organosilanes. J Phys Chem B. 1998;102:5503–10.

33. Mozgawa W. The influence of some heavy metals cations on the FTIR spectra of zeolites. J Mol Struct. 2000;555:299–304.

34. Majdan M, Maryuk O, Gładysz-Płaska A, Pikus S, Kwiatkowski R. Spectral characteristics of the bentonite loaded with benzyldimethyloctadecylammonium chloride, hexadecyltrimethylammonium bromide and dimethyldioctadecylammonium bromide. J Mol Struct. 2008;874(1–3):101–107.

35. Caglar B, Afsin B, Tabak A, Eren E. Characterization of the cation-exchanged bentonites by XRPD. ATR, DTA/TG analyses and BET measurement. Chem Eng J. 2009;149:242–8.

36. Perraki Th, Orfanoudaki A. Mineralogical study of zeolites from Pentalofos area, Thrace, Greece. Appl Clay Sci. 2004;25:9–16.

37. Leite IF, Soares APS, Carvalho LH, Raposo CMO, Malta OML, Silva SML. Characterization of pristine and purified organobentonites. J Therm Anal Calorim. 2010;100:563–9.

38. Saini GSS, Sharma A, Kaur S, Bindra KS, Sathe V, Tripathi SK, Mhahajan CG. Rhodamine 6G interaction with solvents studied

by vibrational spectroscopy and density functional theory. J Mol Struct. 2009;931:10–9.

39. Sarkar J, Chowdhury J, Pal P, Talapatra GB. Ab initio, DFT vibrational calculations and SERRS study of Rhodamine 123 adsorbed on colloidal silver particles. Vib Spectrosc. 2006;41:90–6.

40. Wang L, Roitberg A, Meuse C, Gaigalas AK. Raman and FTIR spectroscopies of fluorescein in solutions. Spectrochim Acta A. 2001;57:1781–91.

41. Önal M, Sarikaya Y. Thermal behavior of a bentonite. J Therm Anal Calorim. 2007;90(1):167–72.

42. Hrachová J, Billik P, Fajnor VS. Influence of organic surfactants on structural stability of mechanochemically treated bentonite. J Thermal Anal Calorim. 2010;101:161–8.

43. Dweck J. Qualitative and quantitative characterization of Brazilian natural and organophilic clays by thermal analysis. J Thermal Anal Calorim. 2008;92:129–35.

44. Lapides I, Yariv S, Golodnitsky D. Simultaneous DTA-TG study of montmorillonite mechanochemically treated with crystal-violet. J Therm Anal Calorim. 2002;67:99–112.

45. Yariv S. The role of charcoal on DTA curves of organo-clay complexes: an overview. Appl Clay Sci. 2004;24:225–36.

46. del Hoyo C, Dorado C, Rodríguez-Cruz MS, Sánchez-Martín MJ. Physico-chemical study of selected surfactant-clay mineral systems. J Therm Anal Calorim. 2008;94:227–34.

47. Tiwari RR, Khilar KC, Natarajan U. Synthesis and characterization of novel organo-montmorillonites. Appl Clay Sci. 2008;38:203–8.

48. Staszczuk P, Sternik D, Kutarov VV. Analysis of the energetic heterogenity of $HgBa_2Ca_2Cu_3O_8 + \delta$ surfaces Q-TG and Q-DTG data. J Thermal Anal Calorim. 2002;69:23–36.